Broadband wide angular response microwave absorbing dielectric resonator array structure

Omar H. AL-Zoubi[1, 2*]

[1]*Renewable Energy Engineering Department, Alalbayt University, Mafrag, Jordan*
[2]*Univeristy of Arkansas, Fayetteville, 72701, AR, USA*

*Corresponding author: Tel: (+96)2798757095; E-mail: oalzoubi@uark.edu

Abstract

In this article, we report a new method for enhancing microwave absorbing material properties by using dielectric resonator arrays structure. The proposed structure is an array of circular cylinder dielectric resonators (CDR) that are composed of microwave absorbing (MA) material. The performance of the proposed structure is studied using numerical electromagnetic methods. The results show that an MA martial performance can be significantly enhanced if constructed in the form of CDR arrays compared with similar thickness flat sheet of counterpart MA material. The band width, thickness, angular response, and absorption strength are significantly enhanced by implementing the introduced method. A well deigned CDR array with height of 4 mm can achieve ~ 13 GH 10-dB bandwidth, with ~45-degree angular response. The introduced MA structures exhibits the wide angular response, up to 45 degrees, for both TE and TM polarizations. Copyright © 2017 VBRI Press.

Keywords: Microwave absorbing materials, dielectric resonator arrays, light trapping.

Introduction

Microwave absorbing (MA) absorbing materials have numerous applications in many fields such as military, communications, and EMI/EMC. The MA materials generally have to meet the following features: (i) low thickness, (ii) broadband width, (iii) wide angular response, (iv) polarization independency, and (v) strong absorption [1]. Unfortunately, meeting all of these requirements simultaneously is a challenging task. In many applications, low thickness, broadband width and wide angular response of MA material and their structure are of great importance, as in military applications. Different approaches have been proposed in literature to enhance the performance MA materials. Some are based on geometry, others on composite materials, and recently using metamaterial structures [2-14]. Such techniques can provide high performance MA materials and structures, but with compromising complexity in fabrication, high thickness, narrow bandwidth, or the high weight [14]. In this work, we propose a technique to design high performance MA structure. Achieving low thickness, light weight, broadband, wide angular response, and easy to fabricate MA structure simultaneously is our focus in this work. Inspired by light trapping techniques that are used in optical applications, we propose using DR array structures that can offer low reflectance, strong absorption, broadband, and wide angular response MA structure.

Light-trapping by using arrays of dielectric materials, as semiconductor nanowire arrays, have been proven to achieve high optical performance [15-17]. Based on already available MA materials, we propose constructing an array of CDR composed from an MA material. The electromagnetic (EM) waves interact with the array in a manner similar to light interaction with light-trapping array structures. Our approach is based on utilizing CDR, which is usually utilized in communication applications as antennas, in the form of array that behaves as MA layer. Up to our knowledge, CDR arrays have not been proposed for usage as MA absorbing structures. Our focus in this work is on utilizing geometry to enhance the performance of the already available MA materials. For this purpose, we selected an MA material with known microwave properties over the range of 1- 18 GHz, and applied the proposed technique to proof the concept. By using the proposed structure in this work, the performance of the already available MA material has been significantly enhanced. The already available MA structures performance, in the form of sheets, foam structures, and pyramidal structures, for example, can be enhanced further by texturing their surfaces in the form of the proposed CDR arrays.

Experimental

Materials

The selected material in this study is a composite MA material with known microwave properties, taken from [19]. This material is originally synthesized to enhance the MA properties by including nonmaterial into in it. In the proposed technique, we utilize this composite material to

construct a CDR array, with elements that are composed from this MA material, as shown in **Fig. (1b).** Worth to mention that this MA material is dispersive material with relative permittivity range of 16-28, in frequency band of 1- 18GHz.
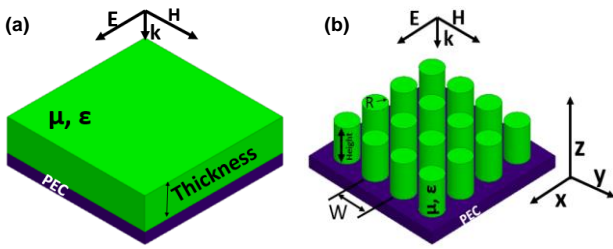

Fig. 1. 3D depiction of a plane MA material and CDR array backed by PEC plane in (a) and (b), respectively.

Numerical modeling and simulation setup

To study the EM interaction with the structure, quantify, and optimize their dimensions for performance, we use numerical electromagnetic methods. The commercial software package, ANSYS HFSS, which offers the capability of simulating subwavelength structures and dispersive materials, is implemented. The scattering parameters method is used to calculate the reflection, transmission and absorption properties of the MA-CDR structures. The proposed arrays are constructed from CDR that are arranged in square lattice structure. The arrays can be considered as 2D infinite arrays in the X and Y dimensions as shown in **Fig. (1b)**. To realize these arrays in the simulation domain, basic unit cell with periodic electric and magnetic boundary conditions are implemented, as shown in supplementary **Fig. 7**. To achieve high accuracy of the computational results, maximum discretization size of the simulation domain has been discretized and set to 10% of the minimum physical dimension of the structure. Supplementary **Fig. 8** shows the convergence analysis of the solution as function of the discretization step size.

Characterizations and response calculations

The performance of the CDR array is quantified by calculating the absorptance of the array as $A(\omega) = 1 - T(\omega) - R(\omega)$, where $T(\omega)$ is the transmittance, and $R(\omega)$ is the reflectance. Scattering parameters methods is used to calculate $T(\omega)$ and $R(\omega)$, where $R(\omega) = |S_{11}(\omega)|^2$ and $T(\omega) = |S_{12}(\omega)|^2$. Due to the fact that the structure is backed by conductive ground plane, the transmittance, $T(\omega)$, equals to zero and the absorptance reduces to $A(\omega) = 1 - R(\omega)$.

Results and discussion

In the case of the flat MA layer backed by a conductor, the interaction of the EM wave with the structure is usually studied theoretically by using transmission line theory. In the structure of flat MA material backed by conductor plane, the reflection loss (RL) is given by [2]:

$$RL = 20 \, log \, |\Gamma| = 20 \, log \left| \frac{\sqrt{\frac{\mu}{\varepsilon}} tanh\left(j\frac{2\pi fd}{c}\sqrt{\mu\varepsilon}\right)-1}{\sqrt{\frac{\mu}{\varepsilon}} tanh\left(j\frac{2\pi fd}{c}\sqrt{\mu\varepsilon}\right)+1} \right| \qquad (1)$$

where Γ is the reflection coefficient, d is the MA layer thickness, μ and ε are the relative permeability and permittivity of the MA material respectively, c the speed of light. One can see the dependence of the RL of the structure on the thickness of the MA layer, d.

In the CDR array, the incident plane EM wave interacts with the array structure in different manner than in plane MA structure. The plane wave couples with a single CDR at certain modes that are governed by different parameters. The analytical solution of Maxwell equations for a single CDR yields an approximation equation that determines the resonance frequencies of this CDR, as [**20**]:

$$\binom{f_{TM_{npm}}}{f_{TE_{npm}}} = \frac{c}{2\pi r\sqrt{\varepsilon\mu}} \sqrt{\left(\frac{X'_{np}}{X_{np}}\right)^2 + \left(\frac{(2m+1)\pi r}{2h}\right)^2} \qquad (2)$$

where, $f_{TM_{npm}}$ is the TM_{npm} mode frequency, $f_{TE_{npm}}$ is the TE_{npm} mode frequency, X'_{np} is the pth root of the nth order Bessel function derivative, X_{np} is the pth root of the nth order Bessel function, r and h are the radius and the height of the CDR respectively. This approximation is valid with reasonable accuracy for single CDR within a specific range of physical dimensions [20]. One can see form Equation (2) that the resonance frequency depends on radius, height and electrical properties of the material. However, the approximation equation for the single CDR can be used in the case of diluted CDR arrays, where the distance between the CDR is large and the mutual coupling between the CDR elements is neglected. In the case of dense array, the mutual coupling between the CDRs are considerable and affects the resonance frequencies of the array structure [**21**]. For this reason, the distance between the CDR elements, lattice constant (LC) of an array, plays a key role in determining the resonance frequency values of an array and its absorption strength. Based on this, for a CDR array that is composed from a certain MA material, the key elements in determining its RL spectrum are the physical dimensions: height, CDR radius, and the LC of the array. The effect of these three parameters have been investigated in this work. Optimization of these parameters for the bandwidth and the absorption strength have been conducted also by parametric analyses. Moreover, normal and oblique incidence of the plane EM wave with parallel and perpendicular polarizations (*TE* and *TM*) have been investigated for optimized arrays.

The height of the CDR array has significant effect on the level of absorption and the resonance frequency as shown in **Fig. 2**. In this figure the, the LC of the array and the CDR radius are set to fixed values. The polarization of the normal incidence plane wave is set to TE polarization. As expected from Equation (2), increasing the height of the CDR decreases the resonance frequency. Two resonance peaks can be seen in the RL spectrum which are attributed to the modes of resonance of the CDR.

To test the effect of the radius of the CDR on the RL spectrum of the array, LC and the height are fixed.

Fig. (3a) shows the spectra of the array at different radii in the range of 1.0 to 2.3 mm.
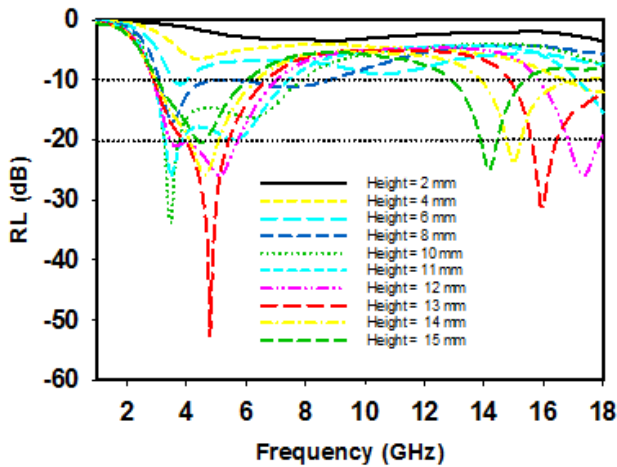

Fig. 2. Reflection loss spectra of the MA-CDR array at different heights with fixed lattice constant of 15 mm and radius of 5 mm.
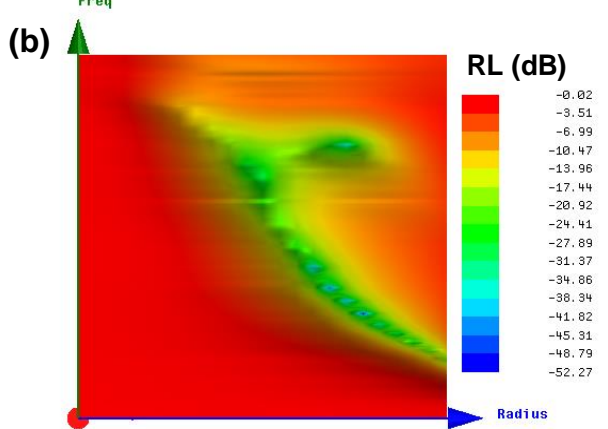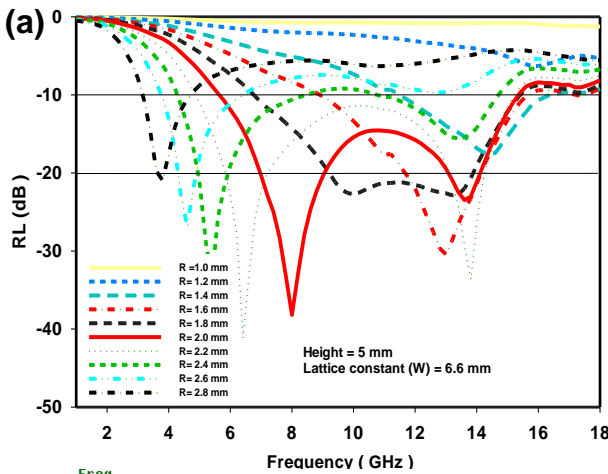

Fig. 3. (a) Reflection loss spectra of the MA-CDR array at different radii with fixed lattice constant of 6.6 mm and height of 5.0 mm. (b) color coded RL values as a function of LC and frequency.

The RL is highly affected by the radius value and one can see that the 10-dB RL bandwidth can reach ~9.0 GHz for the case of 2.4 mm radius. **Fig. (3b)** shows color coded RL value as a function of the CDR radius and frequency. The shift of the peaks in the RL spectrum can be explained

by Equation (2). One can see that a 20-dB bandwidth can reach ~2.5 GHz bandwidth, which means a 99% absorption of EM waves in this band.

Fig. (4a) shows the effect of the LC on the array RL spectrum. One can see that the LC dramatically change the RL peak locations. This effect can be attributed to the wave coupling between the adjacent CDR. By increasing the LC, the peaks shift to higher frequencies. This can be attributed to the coupling modes that occur between the adjacent CDRs. One can see that the LC, for certain height and CDR radius, highly affects the RL bandwidth of the array. For an optimized LC of the array, bandwidth, can reach as high as ~12 GHz in the case of W = 5.6 mm.
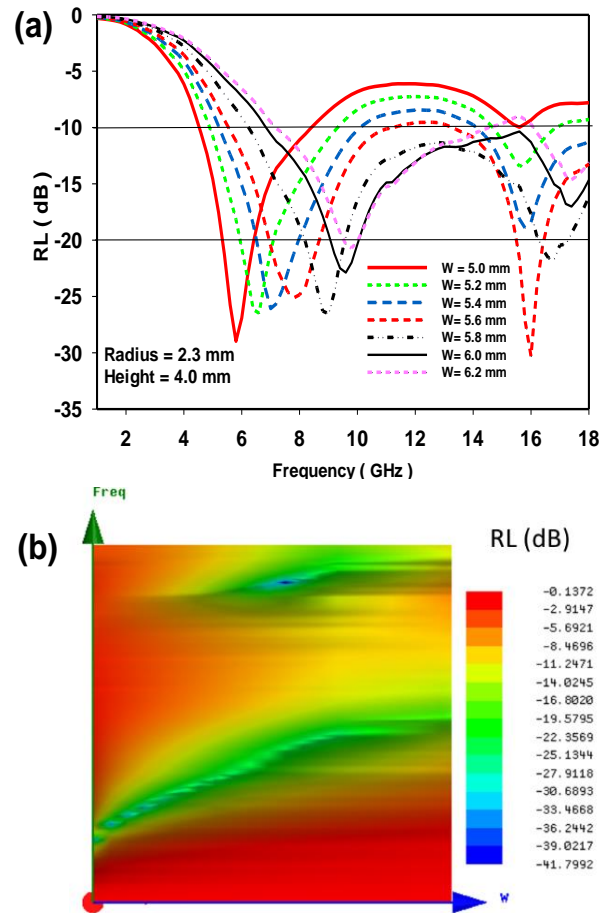

Fig. 4. Reflection loss spectra of the MA-CDR array at different LC with fixed height of 4.0mm and radius of 4.0 mm.

Fig. (4b) demonstrates the effect of increasing the LC on the RL peak value and its location. The coupling between the CDR in the array and its effect is briefly discussed in the supplementary material, where modeling of the array, with invoking some assumptions, is shown in Equation (3).

The performance of the array is highly affected by its three dimension parameters. To obtain optimal performance, parametric analyses is conducted. The results in **Fig. 5** shows the RL spectrum of an optimized array dimensions for the bandwidth. For this array, the 10-dB RL bandwidth is approximately ~13 GHz for CDR radius of 1.9 mm and height of 4.0 mm.
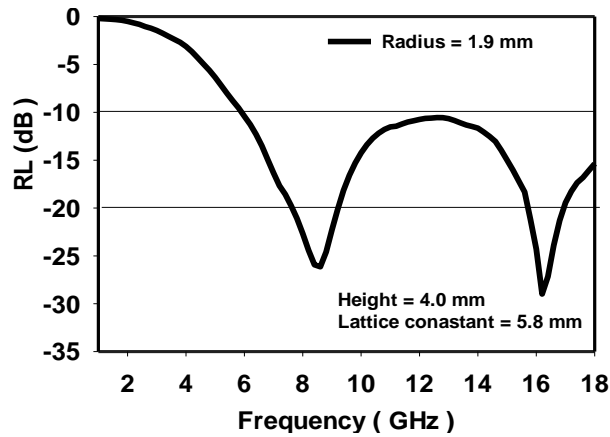
Fig. 5. The RL spectra of optimized dimension MA-CDR arrays for bandwidth.

Another important feature of the MA-CDR array performance is the angular response. For an optimized dimensions array, the angular response is tested for TE and TM polarizations of the incident wave at angles from 0 to 80 degrees off normal, with 5 degrees increment step. **Fig. 6a** shows the RL spectra of the CDR array at different angles of incidence of TE polarized plane wave. One can see that the RL value changes as the angle changes. The strongest absorption, lowest RL, is obtained at 25 degrees, where -46 dB RL is achieved at ~ 8 GHz resonance frequency. The level of RL, at the resonance frequency increases as the angle of incidence increases up to 25 degrees, then it decreases monotonically up to 90 degrees.
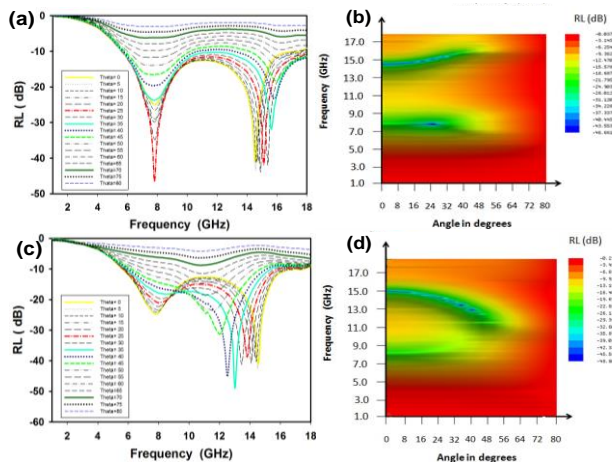

Fig. 6. The RL spectra of an optimized array at different angle of incident of EM plane wave. (a) and (b) are for TE polarized wave (c) and (d) for TM polarized wave.

The RL 10-dB bandwidth slightly changes in the range of 0 to 50 degrees. **Fig. 6b** shows the effect of angle of incidence on the RL level and the shift of the resonance frequencies as a result of angle of incidence. The fundamental mode resonance frequency is slightly changes as the angle of incidence changes. Whereas the higher mode shifts to higher frequency as the angle increases, especially for angles greater than 25 degrees. **Fig. 6c** shows the RL spectra of the array for TM polarized EM wave at

different off normal angles of incidence. In comparison with the TE polarization, the 10-dB bandwidth is almost not affected by the angle of incidence. The level of RL at the fundamental mode is monotonically decreases as the angle increases, whereas the higher mode increases. **Fig. 6d** shows that the higher mode decreases as the angle of incidence increases. Despite this, the 10-dB bandwidth is not highly affected up to 50 degrees. These results show the advantage of the MA-CDR array structure: in addition to the broadband and strong absorption levels, the structure shows independency of angle of incidence and polarization up to 45 degrees of angle of incidence. Interpretation of the obtained results is offered in the supplementary material and the indicated references.
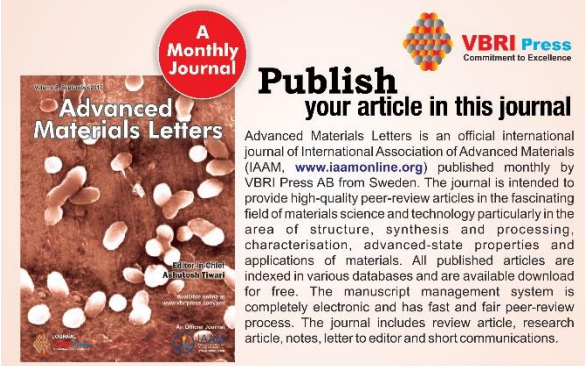
Conclusion

We offer an MA structure in the form of array of CDR. The CDRs are composed of an MA material, and arranged in square-lattice array structures. The microwave performance of the introduced MA-CDR is highly dependent on three parameters of the array physical dimensions. This gives designers three degrees of freedom for tuning the array MA-CDR performance. One finding in this study is that MA-CDR arrays backed by a conductor, compared with the same thickness flat layer of counterpart material, has a significantly enhanced MA performance. Another finding is that the RL spectrum of a certain MA-CDR can be tuned and tailored by manipulating three parameters of the array dimensions. Furthermore, the obtained results show that the proposed MA-CDR arrays has wide angular response that is free of polarization.

All of all, the introduced structure enhances the performance of MA materials in many aspects: Thickness, bandwidth, level of absorption, angular response, and polarization independency. This can be achieved by using geometry without modifying the MA material itself. These results can pave the road for producing ultrathin, broadband, wide angular response MA structures by using noncomplex fabrication techniques.

References

1. Saville, Paul. Defence Research and Development Atlantic, Dartmouth (Canada), **2005**.
2. Qin, F.; Brosseau, C., *J. Appl. Phys.*, **2012**, *111*, 61301.
3. Kaur, R.; Aul, G. D., "Review on microwave absorbing material using different carbon composites," in *International Journal of Engineering Research and Technology*, **2014**, *3*.
4. Melvin, G. J. H.; Ni, Q. Q.; Suzuki, Y.; Natsuki, T., "Microwave-absorbing properties of silver nanoparticle/carbon nanotube hybrid nanocomposites," *J. Mater. Sci.*, **2014**, *49*, 5199.
5. Munir, A., "Microwave Radar Absorbing Properties of Multiwalled Carbon Nanotubes Polymer Composites: A Review," *Adv. Polym. Technol.*, **2015**.
6. B. D. Che, B. Q. Nguyen, L.-T. T. Nguyen, H. T. Nguyen, V. Q. Nguyen, T. Van Le, and N. H. Nguyen, "The impact of different multi-walled carbon nanotubes on the X-band microwave absorption of their epoxy nanocomposites," *Chem. Cent. J.*, vol. 9, no. 1, p. 1, **2015**.
7. P. Savi, M. Miscuglio, M. Giorcelli, and A. Tagliaferro, "ANALYSIS OF MICROWAVE ABSORBING PROPERTIES OF EPOXY MWCNT COMPOSITES," *Prog. Electromagn. Res. Lett.*, **2014**, *44*, 63.

8.   L. Olmedo, P. Hourquebie, and F. Jousse, "Microwave absorbing materials based on conducting polymers," *Adv. Mater.*, **1993**, *5*, 373,

9.   T. McNally and P. Pötschke, *Polymer-carbon nanotube composites: Preparation, properties and applications*. Elsevier, **2011**.

10.   J. J. Pesque, D. P. Bouche, and R. Mittra, "Optimization of multilayer antireflection coatings using an optimal control method," *IEEE Trans. Microw. Theory Tech.*, **1992**, *40*, 1789.

11.   R. W. Wright, "Combined layers in a microwave radiation absorber," Patent, US4012738 A, **1977**.

12.   N. Zhao, T. Zou, C. Shi, J. Li, and W. Guo, "Microwave absorbing properties of activated carbon-fiber felt screens (vertical-arranged carbon fibers)/epoxy resin composites," *Mater. Sci. Eng. B*, **2006**, *127*, 207.

13.   P. Lee, J. Y. Rhee, Y. J. Yoo, K. W. Kim, and others, *Metamaterials for Perfect Absorption*, Springer, **2016**, 236.

14.   C. M. Watts, X. Liu, and W. J. Padilla, "Metamaterial Electromagnetic Wave Absorbers," *Adv. Mater.*, vol. 24, no. 23, p. OP98-OP120, Jun. **2012**.

15.   O. H. A. Zoubi, T. M. Said, M. A. Alher, S. E. Ghazaly, and H. Naseem, "Broadband high efficiency silicon nanowire arrays with radial diversity within diamond-like geometrical distribution for photovoltaic applications," *Opt. Express*, **2015,** 23, A767.

16.   B. Hua, Q. Lin, Q. Zhang, and Z. Fan, "Efficient photon management with nanostructures for photovoltaics," *Nanoscale*, **2013**, 5, 6627.

17.   H.-P. Wang, D.-H. Lien, M.-L. Tsai, C.-A. Lin, H.-C. Chang, K.-Y. Lai, and J.-H. He, "Photon management in nanostructured solar cells," *J. Mater. Chem. C*, **2014**, *2*, 3144.

18.   N. Anttu and H. Q. Xu, "Efficient light management in vertical nanowire arrays for photovoltaics," *Opt. Express*, 2013, 21, A558.

19.   H. Zhao, Z. Zhu, C. Xiong, X. Zheng, and Q. Lin, "The influence of different Ni contents on the radar absorbing properties of FeNi nano powders," *RSC Adv.*, **2016**, *6*, 16413.

20.   C. A. Balanis, Advanced engineering electromagnetics. Chapter 9, John Wiley & Sons, **2012**.

21.   A. Trubin, Lattices of Dielectric Resonators. Springer, 2015.

22.   K. T. Fountaine, W. S. Whitney, and H. A. Atwater, "Resonant absorption in semiconductor nanowires and nanowire arrays: Relating leaky waveguide modes to Bloch photonic crystal modes," *J. Appl. Phys.*, **2014**, *116*, 153106.

23.   B. C. P. Sturmberg, K. B. Dossou, L. C. Botten, A. A. Asatryan, C. G. Poulton, C. M. de Sterke, and R. C. McPhedran, "Modal analysis of enhanced absorption in silicon nanowire arrays," *Opt. Express*, **2011**, *19*, A1067.

24.   Al-Zoubi, Omar H, Hameed Naseem. "*Enhancing the Performance of the Microwave Absorbing Materials by using Dielectric Resonator Arrays,*" *Modelling and Simulation in Engineering*, **2017** no. 3658247, 8 pages.

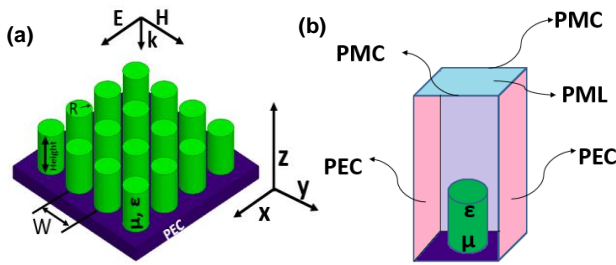## Supporting information

A. Simulation setup:

Fig. 7. depiction of the CDR array backed by condctor palne in (a) , and unit cell with periodic boundary condtions: perfect electric conductor wall, magentic perfrct conductor wall , perfect matching layer, and ground plane in (b).

Fig. 7b shows the set up of the periodic unit cell in the simulation domain for the CDR array backed by a ondutor plane.
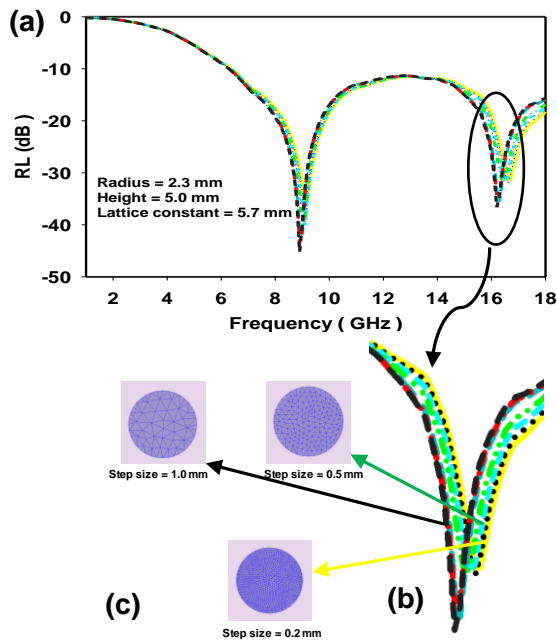

Fig. 8. The RL spectrum of a MA-CDR array calculated at different discretization step sizes (a), Zoomed part of the RL spectrum (b), and top view of the CDR includes the discretization mesh at different discretization levels (c) [24].

B. Convergence Analyses :

In order to obtain reasonable accuracy of the simulation results, using reasonable computational resources, the domain discretization resolution should be set at certain value. For this purposes, we run convergence analysis of the numerical solution at different discretization resolutions. HFSS software uses adaptive meshing algorithm to discretize the 3D simulation domain into tetrahedral sub-elements. The maximum length the tetrahedral edges can be set not to exceed a certain value, which determines the discretization resolution. For the proposed array, we conducted convergence analysis of the

solution at different discretization step sizes. In this analysis, the maximum length of the tetrahedral edges is set to be 0.1 mm up to 1.0 mm, with 0.1 mm increment at each run. The results in **Fig. (8a)** show the RL spectrum of an array of 2.2 mm radius, 5.0 mm height, and 5.7 lattice constant, calculated at different discretization resolutions. **Fig. (8b)** shows a zoomed part of the RL spectrum, where the spectrum lines are corresponded to the discretization level shown in **Fig. (8c)**. A top view of a CDR of 2.2 mm radius at different discretization step sizes is illustrated in **Fig. (8c).** One can see that the solution converges to the resonance frequency at 0.5 mm discretization step size, which is 0.25 % of the CDR radius. However, to guarantee the accuracy of the obtained results for different dimension arrays, we set the maximum discretization step to be 10% of the CDR radius in all of the simulations in this work.

C. Resonance Modes E-filed Distribution

The peaks of the array RL spectra can attributed ot the resonance modes of the CDR composing the array. The values of these resonance frequencies can be predicted roughly by using Equation(2). The CDR in the array excipits E-field distributions that are similar to the modes appear in single CDR. The field distrubtions and the dependance of the resosnce modes on the radius and hieght of the CDR in an array supports the modal interpretation of interaction of EM waves with the array structure.
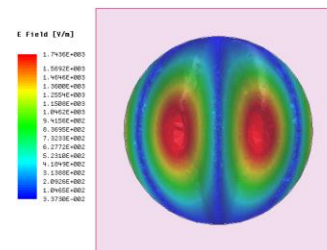
(a)
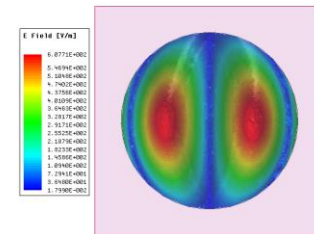
(b)

Fig. 9. Bottom view of te the CDR shows the electric field distribution inside the CDR at the two peaks of the RL spectrum fo the array with dimensions of 2.2 mm radius, 5.0 mm height, and 5.7 lattice constant: (a) at 9.6 GHz, and (b) at 16.6 GHz.

D. Angular Response and Array Approximation Model

This single CDR approximation model can explain and predict absorption peaks of RL of a single CDR with reasonable accuracy. However, it does not take into consideration the mutual coupling between the CDR in an array. Such mutual coupling has impact on the array microwave properties and cannot be neglected, especially

in dense arrays. To take wave coupling in consideration, Fountain *et al.* [22], based on Sturmberg *et al.* [23], introduced a modified eigenvalue equation for infinite arrays of leaky wave guides as:

$$\pm \frac{\beta^2 v^2}{R^2}\left(\frac{1}{\kappa^2}+\frac{1}{\gamma^2}\right)^2 = \left(\frac{J_v'(\kappa R)}{\kappa J_v(\kappa R)} - \frac{H_v'(\gamma R)+S_0 J_v'(\gamma R)}{\gamma H_v(\gamma R)+S_0 J_v(\gamma R)}\right) \tag{3}$$

$$\times \left(\frac{(n_{in}k_0)^2 J_v'(\kappa R)}{\kappa J_v(\kappa R)} - \frac{(n_{out}k_0)^2 H_v'(\gamma R)+S_0 J_v'(\gamma R)}{\gamma H_v(\gamma R)+S_0 J_v(\gamma R)}\right)$$

where κ and γ are the transvers wave vectors inside and outside the CDR, J_v and K_v are Bessel functions of the first and second kinds, β is the wave vector along the CDR axis, R is the CDR radius, v is the order of the Bessel function, n_{in} is the core refractive index, and n_{out} is the outside martial refractive index, H_v is the Hankel function of the vth order, and S_0 represents the nearest neighbor interaction within the lattice. In this approximation, the CDR is treated as leaky wave waveguide.
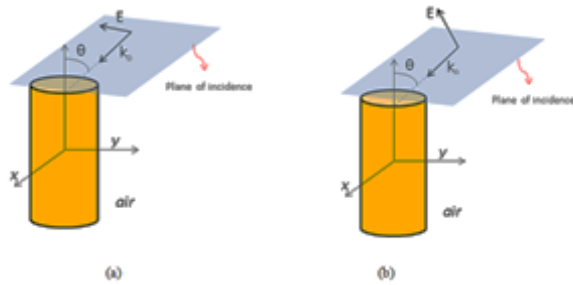

Fig. 9. Demonstration of the off normal incidence of the EM wave with TE and TM polarizations.

By using image theory, the CDR array backed by conductor plane can be modeled by and array of leaky wave guides. In this approach, the mode resonance model explains the strong absorption peaks of the arrays by the coupling of free space plane wave into radial leaky waveguide modes, which are electromagnetic modes with enhanced electric and magnetic field intensities localized inside the CDR. For the off normal angel of incident, the transverse wave vectors inside and outside the CDR can be expressed by $\kappa = k_o\sqrt{n^2-\sin^2(\theta)}$, $\gamma = k_o\sin(\theta)$, and $\beta = k_o\cos(\theta)$, as shown in **Fig. 9**. One can see that the wave vectors are functions of the angle of incidence. Referring back to the transcendental equation, Equation (3), we can see that the arguments of the Bessel functions for normal incidence are $R\kappa$ and $R\gamma$, where R is the CDR radius. For the off normal incidence (θ), these arguments become as $\kappa R = k_o R\sqrt{n^2-\sin^2(\theta)}$ and $R\gamma = Rk_o\cos(\theta)$ [20-22]. The wave vector dependence on the angle of incidence suggests that the excited leaky modes to be different with angle of incidence. Which

explains the shift of resonance peak frequencies as the angle of incidence changes.